JMEPEG (2009) 18:154–161
DOI: 10.1007/s11665-008-9291-8

1059-9495/$19.00

Submerged Arc Stainless Steel Strip Cladding—Effect of Post-Weld Heat Treatment on Thermal Fatigue Resistance

I.C. Kuo, C.P. Chou, C.F. Tseng, and I.K. Lee

(Submitted September 18, 2007; in revised form July 2, 2008)

Two types of martensitic stainless steel strips, PFB-132 and PFB-131S, were deposited on SS41 carbon steel substrate by a three-pass submerged arc cladding process. The effects of post-weld heat treatment (PWHT) on thermal fatigue resistance and hardness were evaluated by thermal fatigue and hardness testing, respectively. The weld metal microstructure was investigated by utilizing optical microscopy, scanning electron microscopy (SEM) equipped with energy dispersive X-ray spectroscopy (EDS) and transmission electron microscopy (TEM). Results showed that, by increasing the PWHT temperature, hardness decreased but there was a simultaneous improvement in weldment thermal fatigue resistance. During tempering, carbide, such as $(Fe, Cr)_{23}C_6$, precipitated in the weld metals and molybdenum appeared to promote $(Fe, Cr, Mo)_{23}C_6$ formation. The precipitates of $(Fe, Cr, Mo)_{23}C_6$ revealed a face-centered cubic (FCC) structure with fine grains distributed in the microstructure, thereby effectively increasing thermal fatigue resistance. However, by adding nickel, the A_{C1} temperature decreased, causing a negative effect on thermal fatigue resistance.

Keywords carbide, hardness, martensitic stainless steel, post-weld heat treatment, submerged arc cladding, thermal fatigue resistance

1. Introduction

Cladding is a process used for developing surfaces with desired properties by depositing a relatively thick layer of filler material on carbon or low-alloy steel base metals (Ref 1-3). Weld cladding generates a very strong metallurgical bond between the surface coating and substrate. Therefore we can recommend the appropriate coating for enhanced corrosion protection, wear resistance or hardness (Ref 4, 5). Martensitic stainless steel alloy coating on low-alloy steel is frequently applied to rolls in continuous casting, hot rolling, and acid pickling in the production of various grades of steel (Ref 6-8). However, when applied at high temperatures, cladding materials suffer cracking or deterioration due to heating/cooling processes, resulting in significant losses of base metals (Ref 9, 10). Therefore, weld metals are heat-treated after welding to improve strength and prolong service life (Ref 11-13).

Gas tungsten arc welding (GTAW), submerged arc welding (SAW), and the more recently developed processes like plasma arc welding (PAW) are widely used for the deposition of welds. It is well known that plasma transferred arc (PTA) hardfacing is an efficient method, using plasma as a heat source and powder as the surface alloy consumable (Ref 14). There are many advantages, such as very high quality deposition, high-energy concentration, narrow heat affected zone, less weld distortion, etc. However, certain disadvantages were noted, namely low deposition rates, overspray, and very high equipment costs (Ref 15, 16). By contrast, SAW cladding offers very high fusion efficiency, compatible with automation, heavy section work, cladding of large areas, resulting in this method being selected in industrial plants (Ref 17). In this study, martensitic stainless steel strips were deposited onto SS41 carbon steel using the SAW cladding process. The effects of post-weld heat treatment (PWHT) on microstructure, hardness, and thermal fatigue resistance were examined.

2. Experimental Methods

Two types of martensitic stainless steel strips, PFB-132 and PFB-131S, were deposited on a SS41 carbon steel substrate by utilizing a submerged arc cladding process. Table 1 presents the chemical composition of various selected materials, with strips size of 0.4 × 50 mm and substrates with dimensions of 270 × 80 × 30 mm. SAW cladding was performed to make three-pass bead-on-plate welds. The preheat and inter-pass temperature for specimens during welding was 250 °C, which was achieved by

Nomenclature	
A_{C1}	temperature at which austenite starts to form

I.C. Kuo and **C.P. Chou**, Department of Mechanical Engineering, National Chiao Tung University, Hsinchu 300, Taiwan; **I.C. Kuo** and **C.F. Tseng**, Department of Materials Science and Engineering, National Formosa University, Yunlin 632, Taiwan; and **I.K. Lee**, Department of Materials Science and Engineering, Dayeh University, Changhua 515, Taiwan. Contact e-mail: ickuo@ms39.hinet.net.

Table 1 Chemical composition of cladding materials and base metal (wt.%)

Material	C	Si	Mn	P	S	Ni	Cr	Mo	Fe
PFB-132	0.065	0.59	1.39	0.022	0.006	2.02	13.47	0.028	Bal.
PFB-131S	0.140	0.68	0.99	0.021	0.011	0.98	12.42	0.37	Bal.
Base metal	0.190	0.13	0.84	0.01	0.007	0.032	0.019	…	Bal.

Table 2 Experimental conditions for submerged arc cladding

Polarity	Current	Voltage	Travel speed	Input energy	Preheat and interpass temperature
DCEP	650 A	24 V	19 cm/min	49 kJ/cm	250 °C

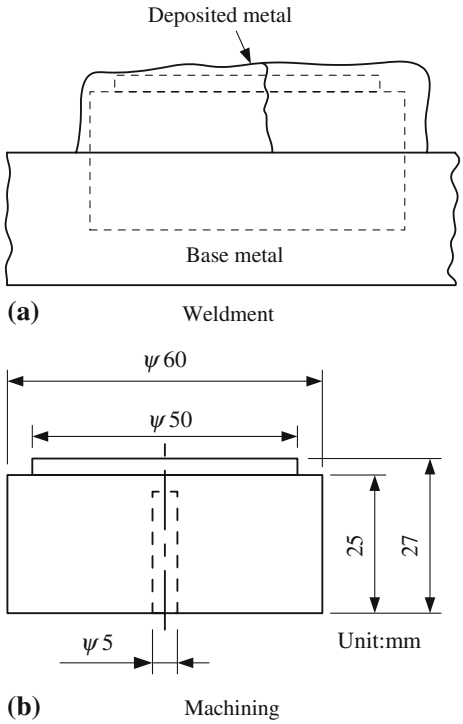

Fig. 1 Dimensions of thermal fatigue specimens

applying a neutral flame. The process parameters are listed in Table 2. Liquid penetrant inspection was used after cladding to detect possible cracking in the weld. Specimens were then heat-treated by the same procedure at temperature of 625, 650, and 675 °C for 2 h and then gradually cooled to room temperature within the furnace. Thermal fatigue properties of the weldments may be significantly affected by the PWHT process and hardness. Hardness of the deposited metal was established by using the Rockwell C scale, utilizing a 120° diamond cone with a 150 kg load. Each reported hardness value was averaged after five measurements.

In the thermal fatigue test, cylindrical-shaped specimens (60 mm diameter and 27 mm thickness) were prepared, and then a hole of 25 mm depth and 5 mm diameter was drilled in the center of each specimen to install k-type thermocouples, as

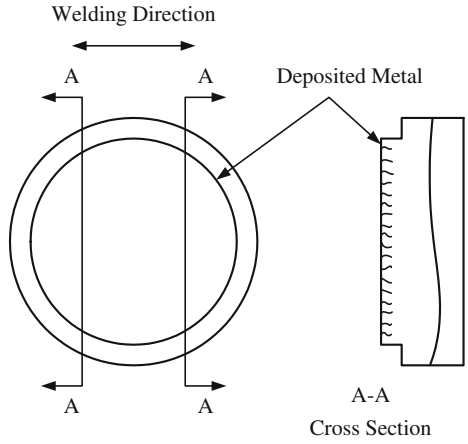

Fig. 2 Observational sketch of thermal fatigue cracks

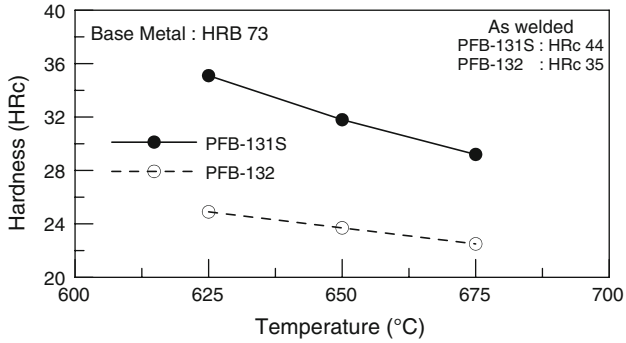

Fig. 3 Relationship between PWHT temperature and the hardness of deposited metal

shown in Fig. 1. Furnace temperature was fixed at 1025 °C. Each test cycle involved heating every specimen to 650 °C in the furnace, and then rapidly cooling with water to 400 °C outside the furnace. After 2000 cycles of thermal testing, edge cracking was discovered on examination. Cracks were inspected using an optical microscope. A schematic diagram of the cracks is depicted in Fig. 2. A section cut from the surface of the deposited metal was used to observe the microstructures of the PWHT weld metals, utilizing a scanning electron microscope (SEM). Energy dispersive X-ray spectroscopy (EDS) was used for the elemental analysis. Transmission electron microscopy (TEM) and selected area diffraction patterns (SADP) were used to investigate microstructures and precipitation phases.

3. Experimental Results and Discussion

3.1 Hardness Analysis

Rockwell hardness measurements of the two sets of specimens (PFB-132 and PFB-131S) are shown in Fig. 3. It can be seen that hardness decreased as temperature increased, and hardness of the PFB-131S specimens was higher than that of the PFB-132 specimen. In general, microstructure and mechanical properties such as hardness are highly dependent upon chemical composition and heat treatment. In other words,

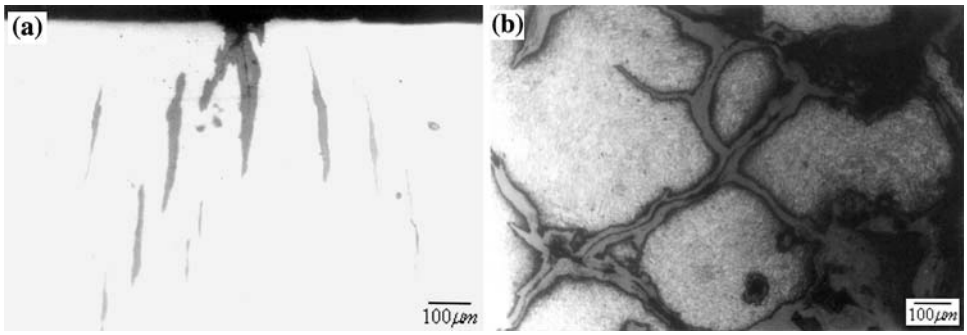

Fig. 4 Optical photographs showing thermal fatigue cracks on the surface of PFB-132: (a) near the corner and (b) near the roll center

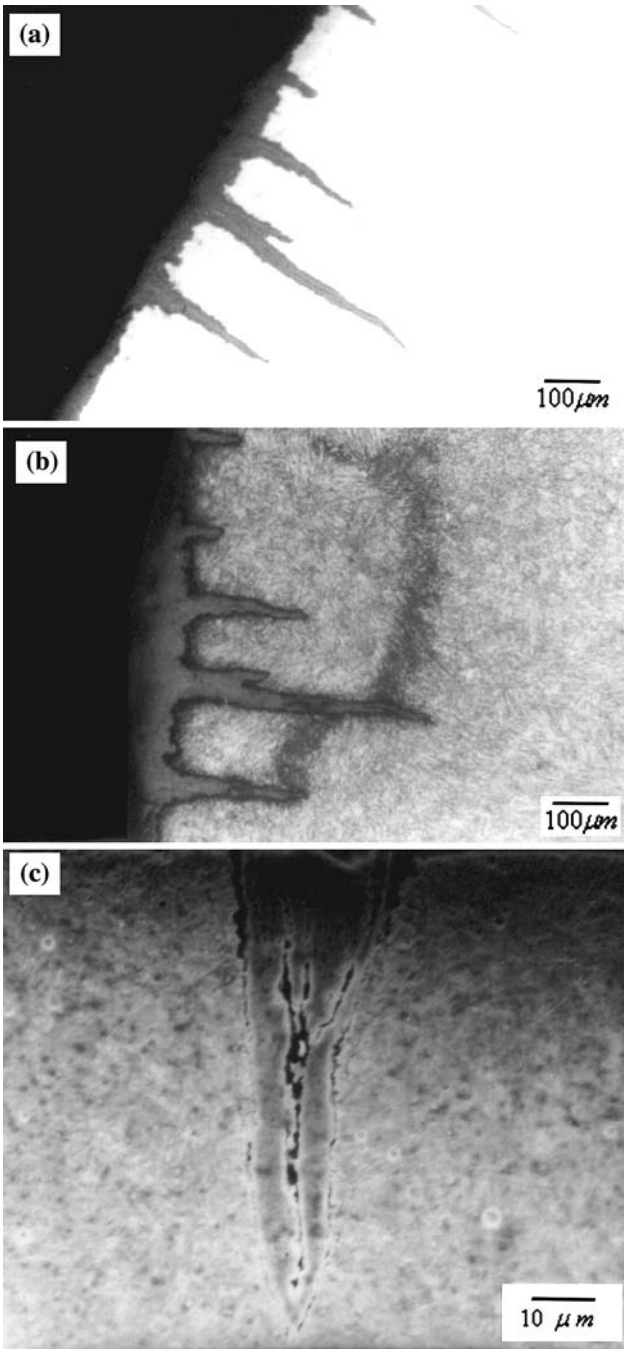

Fig. 5 Photographs of thermal fatigue cracks for A-A cross section of PFB-132: (a) etched, OM; (b) unetched, OM; (c) etched, SEM

Table 3 Thermal fatigue test results

		625 °C	650 °C	675 °C
Total quantity of cracks	PFB-132	97	82	79
	PFB-131S	76	70	67
Total length of cracks, mm	PFB-132	15.82	8.63	8.91
	PFB-131S	3.87	4.25	3.27
Largest crack depth, mm	PFB-132	0.59	0.48	0.47
	PFB-131S	0.10	0.15	0.16

Table 4 Top layers compositions of welded metal (wt.%)

Material	C	Si	Mn	P	S	Ni	Cr	Mo	Fe
PFB-132	0.069	0.596	1.39	0.022	0.011	1.69	13.47	0.028	Bal.
PFB-131S	0.013	0.58	0.98	0.023	0.009	0.87	12.14	0.330	Bal.

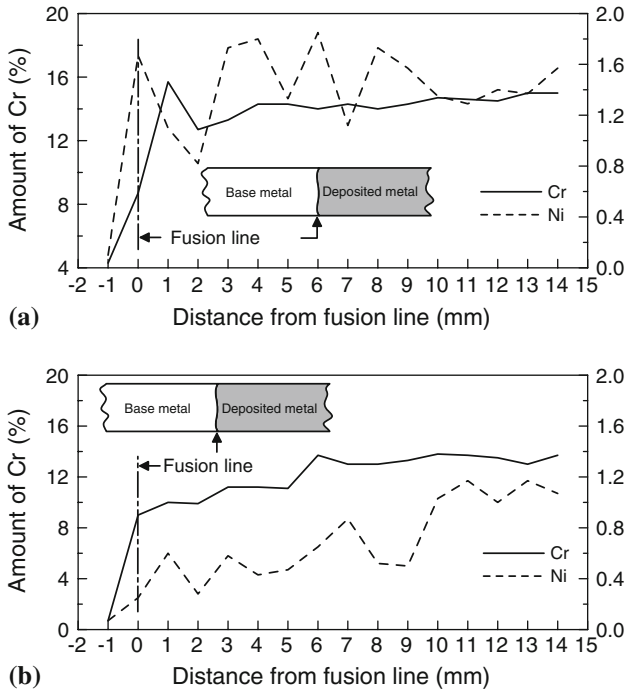

Fig. 6 Changes in quantity of Cr and Ni in the deposited metal: (a) PFB-132 and (b) PFB-131S

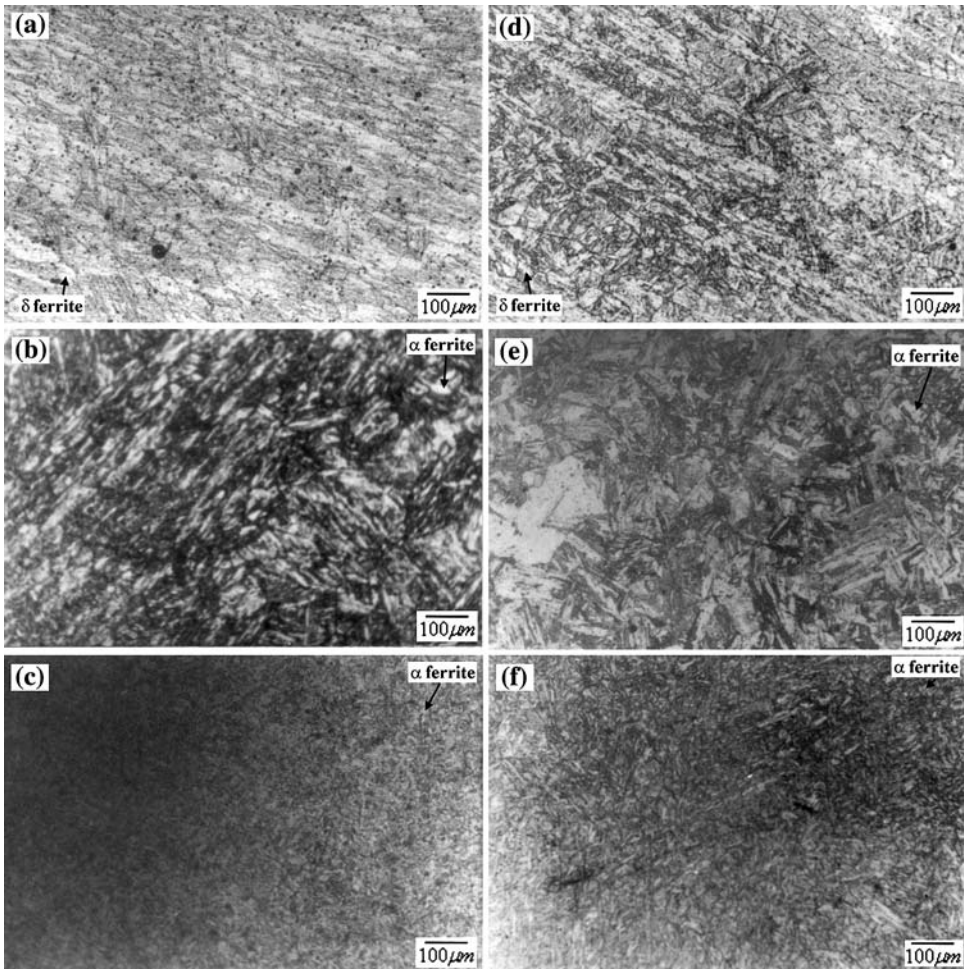

Fig. 7 Microscopic observations of deposited metal: (a) as-welded PFB-132, (b) PFB-132 after tempering at 675 °C, (c) PFB-132 after a thermal fatigue test, (d) as-welded PFB-131S, (e) PFB-131S after tempering at 675 °C, and (f) PFB-131S after a thermal fatigue test

the same heat-treatment conditions were performed on PFB-132 and PFB-131S; the difference in hardness between the two specimens should be caused by differing in chemical compositions.

3.2 Thermal Fatigue Test Results

Cracks near the corner and roll center on specimen surfaces are shown in Fig. 4. The cracks near the corner are worm-like and extend inwards, and a few cracks branch outwards. Cracks near the center displayed a turtle shell pattern. Possibly, the different cracking patterns resulted from stress differences near the specimen corner and center. As the number of thermal cycles increased, pitting tendency also increased.

Figure 5 shows the OM and SEM micrographic images of a selected tested sample. It can be seen that most cracks start and extend from the surface. Two crack types were observed, one of which tapered to a long and very sharp point and the other was short with a dull tip. Cracks with sharp points were formed by a long heating and cooling cycle, and cracks with dull tip were generated under conditions of high heat and humidity. A detailed analysis of crack length, quantity and depth of edge length is shown in Table 3. The total quantity of cracks in the PFB-132 and PFB-131S specimens decreased as the PWHT temperature increased. For the PFB-131S specimens, few changes were observed in the total length of cracks and crack depth. By contrast, the total length of cracks and the crack depth increased as the PWHT temperature decreased in the PFB-132 specimens.

3.3 Chemical Composition Analysis

Table 4 shows the chemical compositions of the top layers for both specimens. PFB-132 had 1.69% Ni, whereas PFB-131S contained 0.87% Ni and 0.33% Mo. Figure 6 shows several changes in quantity of Cr and Ni in the deposited metal. The percentage of Cr and Ni in the second cladding layer remained constant. Chemical composition of the top cladding layer was minimally affected by the base metal.

The PFB-132 specimen contained 1.69% Ni, which was much higher than that in PFB-131S. Several publications explain the A_{C1} temperature decreases in relation to increase in Ni content (Ref 18, 19). The Ni content of the PFB-131S specimen is higher than that of PFB-132, which has a significant temper softening effect. Notably, PFB-131S had 0.33% Mo, thus its precipitation includes Mo carbides. Since Mo is known to be a carbide-former, it is responsible for precipitation hardening by tempering, causing fine carbide precipitates to appear in the structure, which in turn affect the mechanical properties. Therefore, under the same heat-treatment conditions,

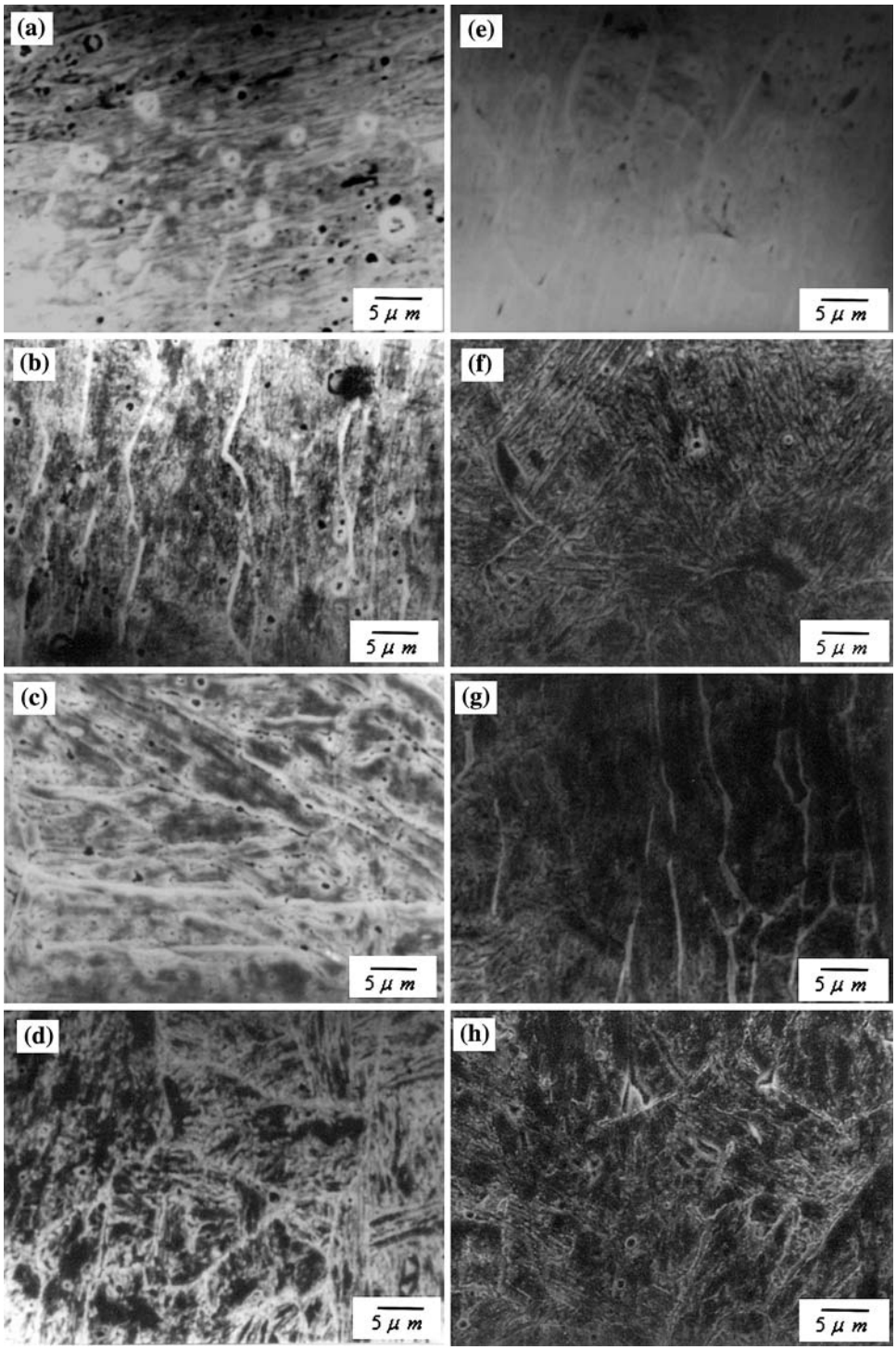

Fig. 8 SEM images of deposited metal: (a) as-welded PFB-132, (b) PFB-132 after tempering at 625 °C, (c) PFB-132 after tempering at 650 °C, (d) PFB-132 after tempering at 675 °C, (e) as-welded PFB-131S, (f) PFB-131S after tempering at 625 °C, (g) PFB-131S after tempering at 650 °C, and (h) PFB-131S after tempering at 675 °C

the hardness of PFB-131S sample was higher than that of the PFB-132 samples.

3.4 Metallographic Analysis

Figure 7 depicts the optical micrographs of specimens PFB-131S and PFB-132. Metals deposited on both specimens had martensitic structures. It was also found that the δ-ferrite phase presented radiation distribution in a martensitic microstructure, as shown in Fig. 7(a) and (d). As PWHT was finished, microstructures revealed decomposing columnar grains forming α-ferrite, as shown in Fig. 7(b) and (e). Furthermore, when the subsequent thermal fatigue test reached 2000 cycles, the decomposition of martensitic structures in both

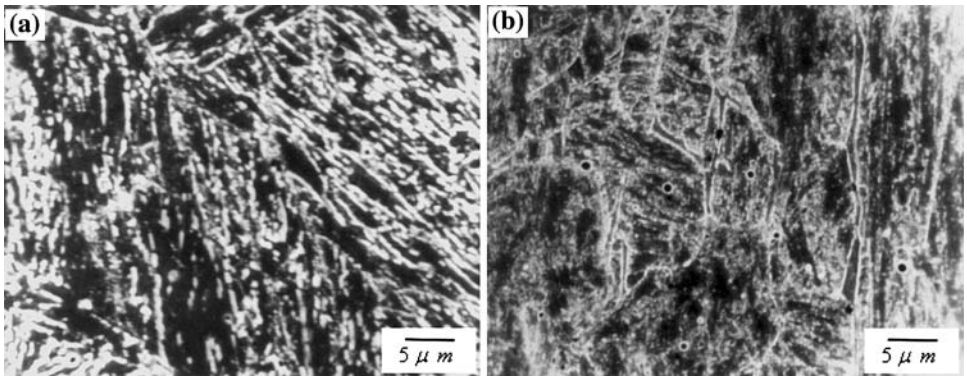

Fig. 9 SEM of deposited metal after thermal fatigue test: (a) PFB-132 and (b) PFB-131S

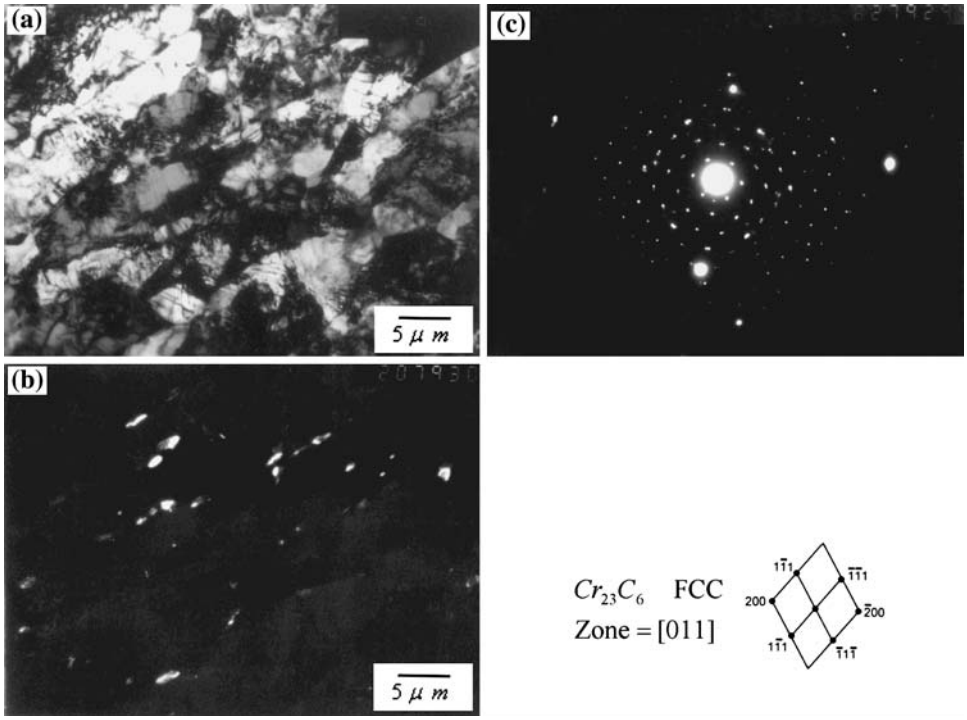

Fig. 10 TEM micrographs of deposited metal of PFB-132 after tempering at 650 °C and thermal fatigue test: (a) bright field image, (b) dark field image, and (c) SADP

specimens was obvious, and the columnar grains decomposed to small uniformly distributed α-ferrite grains, as shown in Fig. 7(c) and (f).

The SEM analysis clearly demonstrated that precipitates had formed on both as-welded specimens. It can be observed that the number of precipitates became more uniform as the heat-treatment temperature increased, as shown in Fig. 8. It was noted that the precipitates of PFB-131S were fine particles, whereas lath-shaped precipitates were observed in the PFB-132 specimen. After completing 2000 thermal cycles, SEM observations demonstrated that the precipitate numbers significantly increased for both specimens. Precipitates of the PFB-132 specimen appear developed along grain boundaries, as shown in Fig. 9. It is well known that precipitates form differently depending on specimen chemical composition. As previously discussed, by increasing the Ni content of the deposited metal, the A_{C1} temperature decreased. Carbides can easily form along the grain boundaries with decreasing A_{C1} temperature. Grain boundaries became weaker, causing a negative effect on thermal cracking resistance. It became apparent that the precipitates increased the effect of stress concentration, resulting in the rapid propagation of crack.

Figure 10-12, respectively, show a TEM bright field, a dark field microstructure, and SADP for samples after continuous thermal fatigue testing. It can be seen that matrices of all specimens revealed a body-centered cubic (BCC) structure, while the precipitates demonstrated a face-centered cubic (FCC) structure. Energy dispersive X-ray (EDX) analysis

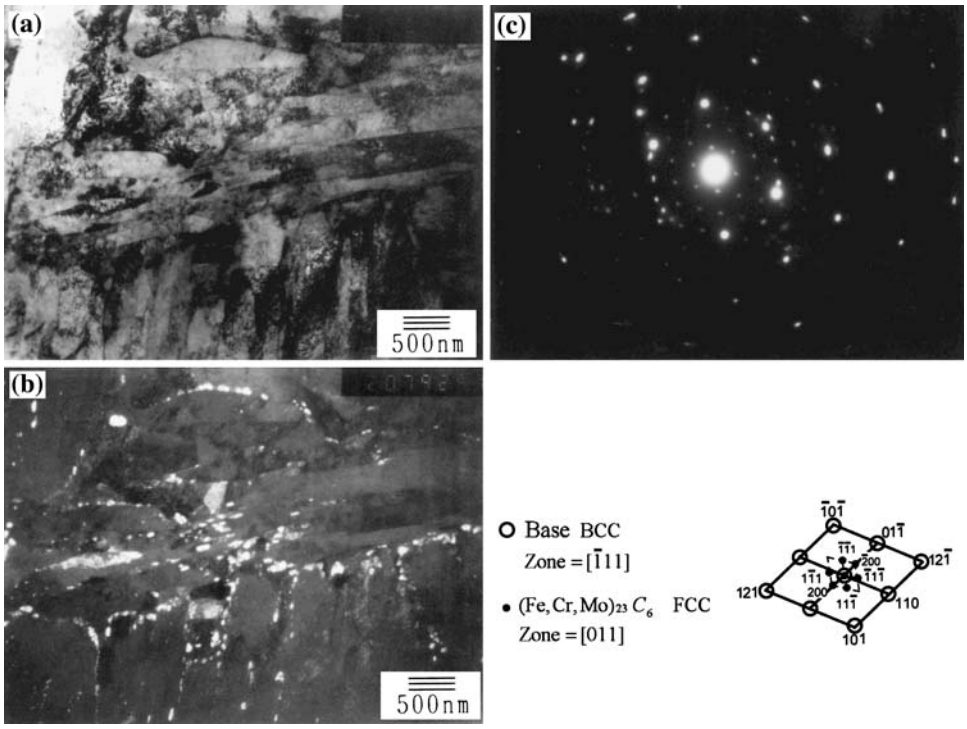

Fig. 11 TEM micrographs for deposited metal of PFB-131S after tempering at 650 °C and thermal fatigue test: (a) bright field image, (b) dark field image, and (c) SADP

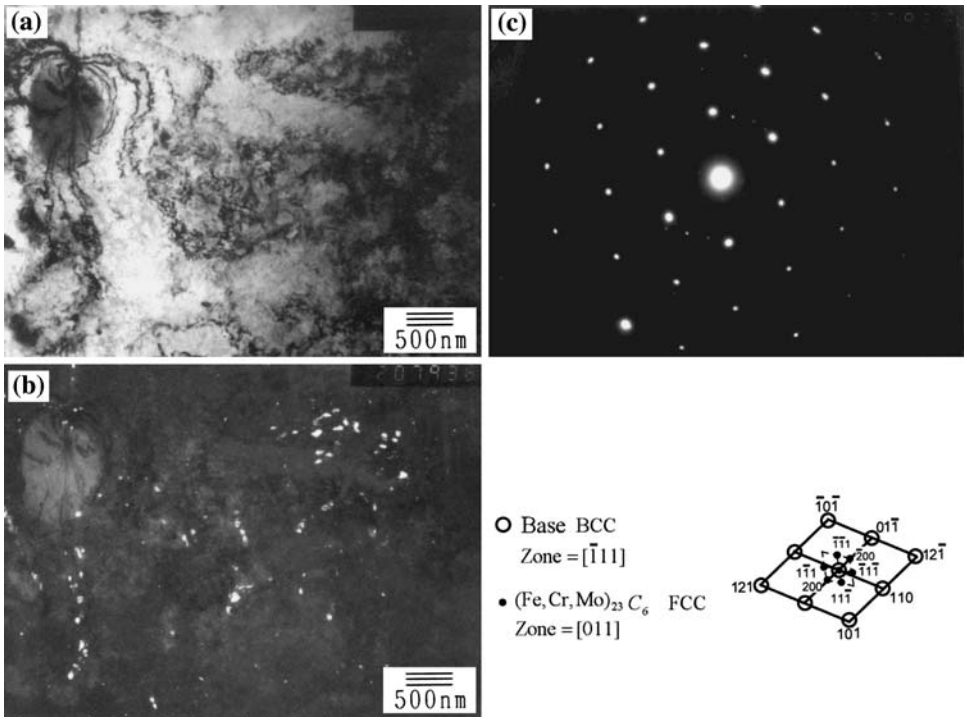

Fig. 12 TEM micrographs of deposited metal of PFB-131S after tempering at 675 °C and thermal fatigue test: (a) bright field image, (b) dark field image, and (c) SADP

clearly show that the precipitates of PFB-132 depicted a chromium-rich FCC $(Fe, Cr)_{23}C_6$ structure, as shown in Fig. 13. Mo carbides precipitation temperature of PFB-131S was lower than that of Cr carbides; therefore, Mo carbides precipitated first at approximately 400 °C and were transformed into $M_{23}C_6$ between 600 and 700 °C (Ref 20, 21). Consequently, the precipitates were found to be complex carbides $(Fe, Cr, Mo)_{23}C_6$.

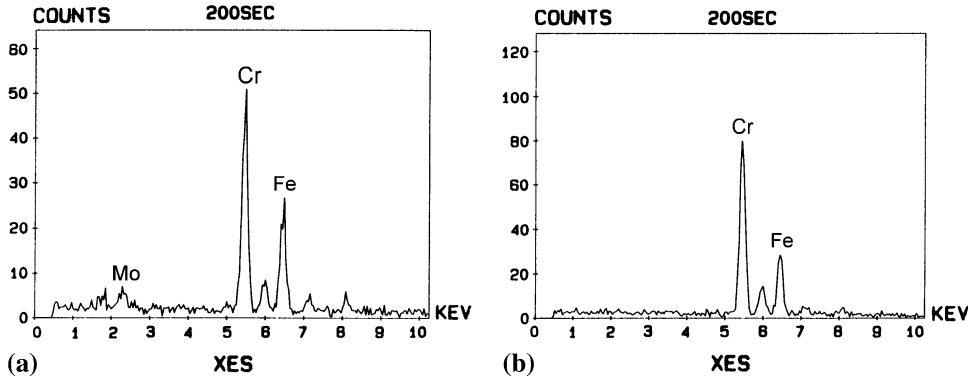

Fig. 13 EDS analysis for the precipitates: (a) PFB-132 and (b) PFB-131S

4. Conclusion

From this study, the following conclusions can be drawn:

1. Hardness was reduced by increasing the PWHT temperature. The hardness of the PFB-131S specimens was higher than that of the PFB-132 specimens.
2. Carbides of (Fe, $Cr)_{23}C_6$ and (Fe, Cr, $Mo)_{23}C_6$ were observed in PFB-132 and PFB-131S specimens. The quantity of (Fe, Cr, $Mo)_{23}C_6$ complex carbides present in the PFB-131S specimens is associated with the presence of molybdenum in the deposited metal.
3. Increasing the Ni content of PFB-132 decreased the A_{C1} temperature of material and promoted temper softening. Carbides developed along the grain boundaries in lath-shaped form, weakening the grain boundaries, and resulting in reduced thermal fatigue resistance.
4. Increasing Mo content of PFB-131S enhanced the number of precipitates of Mo carbides, which developed at low temperatures. Mo carbide precipitations were abundant and fine, resulting in higher thermal fatigue resistance.

References

1. D.W. Gandy, S.J. Findlan, and R. Viswanathan, Weld Repair of Steam Turbine Casings and Piping—An Industry Survey, *ASME J. Press. Vess. Technol.*, 2001, **123**(2), p 157–160
2. A. Bishop, Weld Repairs to High-Pressure Feed/Effluent Heat Exchangers, *Int. J. Press. Vess. Pip.*, 2000, **77**(2–3), p 139–145
3. J.R. Davis, Davis and Associates, Hardfacing, Weld Cladding and Dissimilar Metal Joining. *ASM Handbook-Welding, Brazing and Soldering*, vol. 6, 10th edn., ASM Metals Park, OH, 1993, p 699–828
4. K.G. Budinski, Hardfacing: An Overview of the Processes, *Weld. Des. Fabr.*, 1986, July, p 51–57
5. S. Chatterjee and T.K. Pal, Weld Procedural Effect on the Performance of Iron Based Hardfacing Deposits on Cast Iron Substrate, *J. Mater. Process. Technol.*, 2006, **173**(1), p 61–69
6. P. Corengia, F. Walther, G. Ybarra, S. Sommadossi, R. Corbari, and E. Broitman, Friction and Rolling-Sliding Wear of DC-Pulsed Plasma Nitrided AISI 410 Martensitic Stainless Steel, *Wear*, 2006, **260**(4–5), p 479–485
7. C.X. Li and T. Bell, Corrosion Properties of Plasma Nitrided AISI 410 Martensitic Stainless Steel in 3.5% NaCl and 1% HCl Aqueous Solutions, *Corros. Sci.*, 2006, **48**(8), p 2036–2049
8. B. Gulenc and N. Kahraman, Wear Behaviour of Bulldozer Rollers Welded Using a Submerged Arc Welding Process, *Mater. Des.*, 2003, **24**(7), p 537–542
9. A.K. Bhaduri, T.P.S. Gill, S.K. Albert, K. Shanmugam, and D.R. Iyer, Repair Welding of Cracked Steam Turbine Blades Using Austenitic and Martensitic Stainless-Steel Consumables, *Nucl. Eng. Des.*, 2001, **206**(2–3), p 249–259
10. A.G. Olabi and M.S.J. Hashmi, Effects of the Stress-Relief Conditions on Martensite Stainless-Steel Welded Component, *J. Mater. Process. Technol.*, 1998, **77**(1), p 216–225
11. Y.C. Lin and S.C. Chen, Effect of Residual Stress on Thermal Fatigue in a Type 420 Martensitic Stainless Steel Weldment, *J. Mater. Process. Technol.*, 2003, **138**(1), p 22–27
12. M.C. Tsai, C.S. Chiou, J.S. Du, and J.R. Yang, Phase Transformation in AISI 410 Stainless Steel, *Mater. Sci. Eng. A*, 2002, **332**(1), p 1–10
13. P.D. Bilmes, C.L. Llorente, and M. Solari, Effect of Post Weld Heat Treatments on the Microstructure and Mechanical Behaviour of 13Cr-4NiMoL and 13Cr-6NiMoL Weld Metals, *Proc. 18th Heat Treat. Soc. Conf.*, ASM International, Rosemont, USA, 1998, p 454–463
14. J.N. Aoh and J.C. Chen, On the Wear Characteristics of Cobalt-Based Hardfacing Layer After Thermal Fatigue and Oxidation, *Wear*, 2001, **250**, p 611–620
15. A.S.C.M. D'Oliveira, R.S.C. Paredes, and R.L.C. Santos, Pulsed Current Plasma Transferred Arc Hardfacing, *J. Mater. Process. Technol.*, 2006, **171**, p 167–174
16. A.S. Shahi and S. Pandey, Effect of Auxiliary Preheating of the Filler Wire on Quality of Gas Metal Arc Stainless Steel Claddings, *J. Mater. Eng. Perform.*, 2008, **17**, p 30–36
17. S.-P. Lu, O.-Y. Kwon, T.-B. Kim, and K.-H. Kim, Microstructure and Wear Property of Fe-Mn-Cr-Mo-V Alloy Cladding by Submerged Arc Welding, *J. Mater. Process. Technol.*, 2004, **147**, p 191–196
18. P.D. Bilmes, M. Solari, and C.L. Llorente, Characteristics and Effects of Austenite Resulting from Tempering of 13Cr-NiMo Martensitic Steel Weld Metals, *Mater. Charact.*, 2001, **46**(4), p 285–296
19. T.G. Gooch, Heat Treatment of Welded 13%Cr-4%Ni Martensitic Stainless Steels for Sour Service, *Weld. J.*, 1995, **74**(7), p 213s–223s
20. K.W. Andrews, Empirical Formulae for Calculation of Some Transformation Temperature, *Jpn. Iron Steel Inst.*, 1965, **203**(6), p 721–727
21. C. García de Andrés, G. Caruana, and L.F. Alvarez, Control of $M_{23}C_6$ Carbides in 0.45C-13Cr Martensitic Stainless Steel by Means of Three Representative Heat Treatment Parameters, *Mater. Sci. Eng. A*, 1998, **241**(1), p 211–215